Interacting bosons on a Su-Schrieffer-Heeger ladder: Topological phases and Thouless pumping

Ashirbad Padhan,[1,2,3] Suman Mondal [,4] Smitha Vishveshwara,[5] and Tapan Mishra [2,3,*]

[1]*Department of Physics, Indian Institute of Technology, Guwahati, Assam 781039, India*
[2]*School of Physical Sciences, National Institute of Science Education and Research, Jatni 752050, India*
[3]*Homi Bhabha National Institute, Training School Complex, Anushaktinagar, Mumbai 400094, India*
[4]*Institute for Theoretical Physics, Georg-August-Universität Göttingen, Friedrich-Hund-Platz 1, 37077 Göttingen, Germany*
[5]*Department of Physics, University of Illinois at Urbana-Champaign, Urbana, Illinois 61801, USA*

We study the topological properties of hardcore bosons on a two-leg ladder consisting of two Su-Schrieffer-Heeger chains that are coupled via hopping and interaction. We chart out the phase diagram for the system and show that based on the relative hopping dimerization pattern along the legs, distinctly different topological phases and phase transitions can occur. When the dimerization along the legs is uniform, we find that the topological nature vanishes for even the slightest rung hopping. For staggered dimerization, the system exhibits a well-defined topological character and a topological phase transition as a function of rung hopping. While the topological phase shows bond order character, the trivial phase shows the behavior of a rung-Mott insulator. For this case, the topological nature is found to survive even in the presence of finite interleg interactions. Moreover, we find that the critical point of the topological phase transition shifts to a higher or a lower rung hopping strength depending on the attractive or repulsive nature of the interaction. To highlight the marked effects of interactions, we propose a scheme involving a Thouless charge pump that provides insights for the topological phases characterized by a quantized particle transport through a periodic modulation of appropriate system parameters. In our studies, we show an interaction-induced charge pumping following specific pumping protocols in the case of staggered dimerization.

DOI: 10.1103/PhysRevB.109.085120

I. INTRODUCTION

In the past decade, a profusion of solid-state, ultracold-atomic, and metamaterial systems have realized topological phases of matter that beautifully conform to predictions made at the single-particle level. One of the earliest topological models proposed in the late 1970s in the context of polymers, i.e., the Su-Schrieffer-Heeger (SSH) model [1,2], has formed a paradigm for extensive studies. The SSH model is a tight-binding model of lattice fermions having dimerized hopping and it has offered the simplest platform to realize a topological phase transition in low-dimensional lattice systems [3,4]. Particularly, the SSH model exhibits a topological phase transition from one gapped phase to another as a function of the nearest-neighbor hopping dimerization strength. Topological phases are characterized by zero-energy midgap states corresponding to robust, topologically protected edge bound states in finite geometries. Underlying symmetries that protect the topological character of the phases have attracted recent attention for fundamental physics as well as technological applications [5–11]. The SSH model is now a frontrunner for realization in disparate experimental systems, revealing the signature edge states and distinct topological phase transitions [12–19].

With well-established single-particle topological physics in place, attention has now turned to interaction effects. Here, the nature of the intrinsic particles becomes highly germane: fermions and bosons can both form insulators either due to band effects, and related topology, or due to interactions and Mott physics. Delocalized behavior is typically metal-like in fermions and superfluid in bosons. Quantum particles apart, in metamaterials, excitations could correspond to a variety of features, such as lattice distortions; deviations beyond the lowest order would give rise to effective interactions between these modes. Naturally, the SSH model has formed a key subject for understanding how interactions modify its predicted topological phases [20]. Interparticle interactions in the SSH model and its variants are known to have significant effects on the topological character. In this context, interaction effects have been studied in stabilizing topological phases in a one-dimensional SSH model of few and many interacting particles [21–38]. Moreover, interactions can even induce a topological phase and an associated phase transition [39–41]. Interaction effects have also been generalized to two-component systems in the framework of the SSH-Hubbard model [22,26,27,42–47]. On the experimental front, the topological phases have been observed in a one-dimensional interacting SSH model [48] and also in an SSH-Hubbard model [49]. While the topological properties of the SSH model in the presence of interaction has been a topic of great interest in recent years due to their accessibility in experiments involving artificial systems such as ultracold atoms in optical lattices, the physics of coupled SSH chains is still not well explored.

In this theoretical work, we investigate the interplay between interactions and interchain coupling in the case of
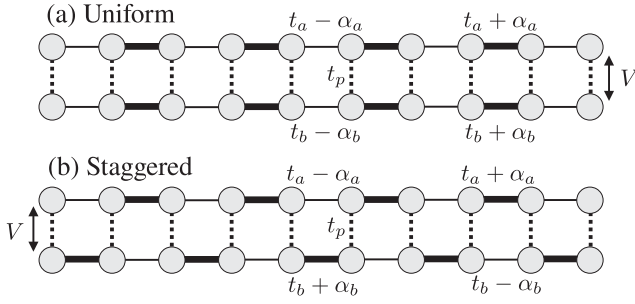
*mishratapan@gmail.com

FIG. 1. Two-leg ladder with different hopping dimerization patterns: (a) the uniform dimerization pattern and (b) the staggered dimerization pattern. t_a, t_b, and t_p are the hoppings along leg a, leg b, and along the rungs of the ladder. α_a and α_b decide the dimerization along leg a and leg b, respectively. The circles represent the sites, and the thick (thin) bonds along the legs represent the strong (weak) hopping strengths. The dashed vertical lines illustrate the rung hopping. We allow interparticle interaction V only along the rungs, which is marked by the arrow.

multiple SSH chains, and its effect on topological physics. As depicted in Fig. 1, two-leg ladders provide a minimal setup to explore the intermediate regime between one- and two-dimensional lattices. The topological properties of these coupled SSH models have been theoretically investigated at the single-particle level [50–59] and even realized experimentally [60]. The coupling between the chains, which forms the ladder, provides a degree of freedom to vary, and the possibility of new phases. In particular, if the dimerization pattern is uniform between chains [Fig. 1(a)], the smallest amount of rung coupling renders topology to be weak. In that case, edge states between chains can hybridize and break away from their zero-energy status. If the dimerization pattern is staggered between chains [Fig. 1(b)], such rung hopping can result in three phases [53]. Two of the phases entail having topologically protected midgap states, as would be found in individual chains. A third, also gapped, phase results from strong enough coupling between chains such that the midgap states completely disappear, and only bulk states exist. The effect of interactions on this physics has been studied in many-body spin and fermionic systems [61,62]. Many-body physics in bosonic SSH ladders is far from a simple extrapolation; competing effects, such as superfluidity, offer widely unexplored regimes and form the subject of our study.

In this paper, we thus perform an in-depth study of the topological nature of hardcore bosons on the two-leg SSH ladder in the presence of interleg interactions. We first review single-particle physics to set the stage for phenomena exhibited by interacting bosons. We establish how the most significant effects of topology come into play at half filling, away from gapless superfluid phases that surround gapped phases in parameter space. On introducing interleg interactions, for the uniform ladder, we show how a rung-Mott insulator phase can dictate and suppress the topological nature of the system. For the staggered ladder, starting from a topological phase at a fixed rung hopping, we show that the system sustains a robust topological phase with increasing interleg interactions until it reaches a critical strength at which it undergoes a phase transition to a trivial phase. We find that

the topological phase transition is sensitive to the nature of the interaction, i.e., a topological to trivial phase transition occurs at a smaller (larger) critical rung hopping when the interaction is repulsive (attractive). We do a careful study to quantify these topological properties by deriving and analyzing the excitation spectrum, finite edge polarization, quantized Berry's phase, and Thouless charge pumping properties. Our studies show that the SSH bosonic ladder has a rich range of phases, is topologically robust, and has some features that are markedly different from its single-particle and fermionic counterparts.

The paper is organized as follows. In Sec. II, we discuss the model and the method used for our studies. We obtain the single-particle spectrum in Sec. III, and employ it in Sec. IV to derive results pertaining to the many-body hardcore bosonic system in the absence of interleg interactions. In Sec. V, we perform an involved analysis of the behavior of the SSH ladder in the presence of interleg interactions, concluding with a derivation and discussion of Thouless charge pumping. Finally, in Sec. VI, we provide a summary and outlook.

II. MODEL AND APPROACH

The systems of interacting hardcore bosons on a two-leg SSH ladder studied here are described by the Hamiltonian

$$
\begin{aligned}
\mathcal{H} = &- \sum_j [t_a - (-1)^j \alpha_a](a_j^\dagger a_{j+1} + \text{H.c.}) \\
&- \sum_j [t_b - (-1)^j \alpha_b](b_j^\dagger b_{j+1} + \text{H.c.}) \\
&- t_p \sum_j (a_j^\dagger b_j + \text{H.c.}) + V \sum_j n_{aj} n_{bj}, \quad (1)
\end{aligned}
$$

where $a_j(b_j)$ and $n_{aj}(n_{bj})$ are, respectively, the bosonic annihilation and on-site number operator for the jth lattice site on leg $a(b)$. The hopping amplitudes along the respective legs are denoted by t_a and t_b. The parameters α_a and α_b set the SSH-model-type dimerization along the a and b legs, respectively. The two legs interact with each other through hopping and interactions along the rung direction. Here, t_p represents the hopping amplitude along the rung, and V is the interleg interaction strength. The hardcore constraint is imposed by assuming $(a^\dagger)^2 = 0$, which ensures not more than one boson in a particular site.

Note that in the absence of both interaction ($V = 0$) and rung hopping ($t_p = 0$), the model considered above transforms to two decoupled legs whose physics solely depends on the choice of dimerization, i.e., α_a and α_b. At half filling of hardcore bosons, the two chains exhibit topological or trivial character, when the dimerizations α_a and α_b are considered to be both positive or both negative. This indicates a topological phase transition as the dimerizations vary from negative to positive values, or vice versa. Additionally, in the absence of dimerization, i.e., $\alpha_a = \alpha_b = 0$, the noninteracting version ($V = 0$) of $\mathcal{H}$ is known to exhibit a rung-Mott insulator (RMI) phase for any finite values of rung hopping t_p where a particle tries to localize in each rung [63]. However, the combined effect of dimerization, rung hopping, and interaction in such many-body system is not well explored.

In this work, we systematically analyze the effect of t_p and V on the topological properties of the system. In our studies, we consider two different combinations of dimerizations such as (a) uniform dimerization, i.e., $\alpha_a = \alpha_b > 0$, and (b) staggered dimerization, i.e., $\alpha_a = -\alpha_b > 0$, as depicted in Figs. 1(a) and 1(b), respectively. In the absence of t_p and V, for the uniform dimerization case, the particles in both the legs are in topological phases, and for the staggered dimerization case, the particles in leg a are in a topological phase and in leg b they are in the trivial phase. In the following, we study the effect of t_p and V on the topological features of the system.

To achieve the above two dimerization patterns, we set the following parameters. The uniform dimerization is enforced by fixing $t_a = t_b = t$ and $\alpha_a = \alpha_b = \alpha$. Similarly, the staggered dimerization pattern along the legs is enforced by setting $t_a = t_b = t$ and $\alpha_a = -\alpha_b = \alpha$. We consider $t = 0.6$ and $\alpha = 0.4$ in our calculations such that the hopping strength in the strong and weak bonds in the legs is $t_1 = t + \alpha = 1$ and $t_2 = t - \alpha = 0.2$, respectively. Here, $t_1 = 1.0$ defines the unit of energy, which makes the other parameters in the system dimensionless. These choices of parameters make the system strongly dimerized in the decoupled limit ($t_p = V = 0$), where the topological properties are very prominent such as the edge states with very small correlation length (well localized) and large bulk gap.

We numerically obtain the ground-state properties of the system using the density matrix renormalization group (DMRG) method [64,65] based on the matrix product states (MPS) approach [66,67]. We consider a ladder of length up to $L = 100$ rungs (i.e., 200 sites) for different particle number sectors of N hardcore bosons with the desired densities $\rho = N/2L$. Unless otherwise mentioned, we compute the physical quantities in the thermodynamic limit ($L = \infty$) by using the appropriate extrapolation technique to minimize finite-size effects. The accuracy of the DMRG simulations is ensured by considering sufficiently large bond dimensions (χ) up to $\chi = 500$.

III. SINGLE-PARTICLE SPECTRUM

Before presenting many-body features, we first analyze the single-particle spectrum of the model shown in Eq. (1). Although the model under consideration is for hardcore bosons, we show that significant insights about the topological properties of the many-particle ground state can be obtained from the single-particle spectrum at different fillings. In the following, we describe the quantum phases at different fillings for both the uniform and staggered dimerization configurations considered in our study.

As a specific representative case, we plot the numerically obtained single-particle spectrum as a function of t_p for a system of length $L = 20$ for uniform dimerization case ($t_a = t_b = 0.6t_1$ and $\alpha_a = \alpha_b = 0.4t_1$) and staggered dimerization case ($t_a = t_b = 0.6t_1$ and $\alpha_a = -\alpha_b = 0.4t_1$) in Figs. 2(a) and 2(b), respectively. Note that for the case of uniform dimerization, the system is a weak topological system consisting of a stack of lattices that are topologically identical in nature. When $t_p = 0$, the two legs of the ladder are equivalent to two isolated SSH chains, which are individually known to manifest a gap in the middle of the spectrum due to the onset of the bond
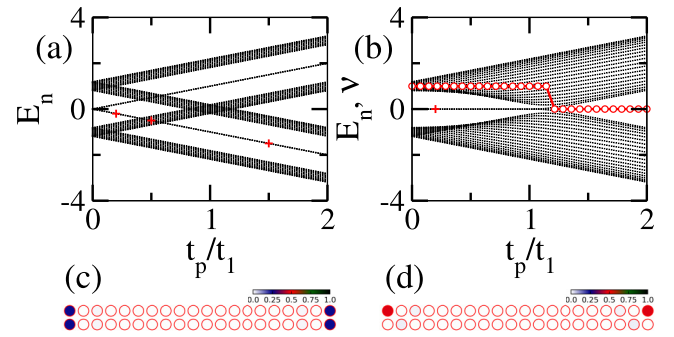

FIG. 2. The single-particle energy spectrum of a system of 40 sites ($L = 20$) with varying t_p for (a) uniform dimerization pattern ($t_a = t_b = 0.6t_1$ and $\alpha_a = \alpha_b = 0.4t_1$) and (b) staggered dimerization pattern ($t_a = t_b = 0.6t_1$ and $\alpha_a = -\alpha_b = 0.4t_1$) along the legs. The red line with circles in (b) denotes the corresponding winding number ν. (c),(d) The on-site probability $|\psi_j|^2$ of states marked by the red plus signs in (a) and (b), respectively. Note that the on-site probability for all the states marked in (a) is identical to that in (c). This clearly indicates that the edge states are crossing the band from one gapped phase to another.

order (BO) phase [23]. This gapped phase hosts a pair of symmetry-protected zero-energy edge states [see Fig. 2(a)]. When t_p takes finite values, apart from the gap at the middle of the spectrum, two more gaps open up symmetrically at one-quarter and three-quarter fillings of the spectrum after a critical t_p due to the formation of a plaquette order (PO) in the system, which will be discussed in detail in the next section. The zero-energy edge modes in the two legs of the ladder hybridize to become energetic while staying at the edges. These states can be called midgap states. However, in this case, these states merge with the energy bands before the bulk gap closes at a higher value of t_p, violating the bulk-edge correspondence. As mentioned before, this phenomenon can be attributed to the weak topology of the uniform dimerization configuration. With further increase in t_p, the bulk gap opens up again but without the midgap states. A pair of midgap states appears inside the two symmetrically formed gaps at one-quarter and three-quarter fillings of the energy spectrum. To confirm that these midgap states are edge states, in Fig 2(c) we plot the probability density $|\psi_j|^2$ of these states marked by red plus signs in Fig. 2(a), where ψ_j is the wave-function amplitude at each lattice site j. It can be clearly seen that the amplitude ψ_j has maximum weight on the edge lattice sites of both the legs. We note that these midgap states cross the bulk bands and go from one gapped phase to another gapped phase as a function of t_p. While crossing the band, the edge state retains its properties, i.e., the probability density behaves similar to Fig. 2(c) at all three positions marked by the red plus symbols in Fig. 2(a).

For the case of staggered dimerization, however, the single-particle spectrum exhibits a simple but topologically richer picture. In this case a gap-closing transition occurs between two gapped phases as a function of t_p, where one of the gapped phases hosts zero-energy edge modes, as can be seen from Fig. 2(b). We plot the probability density ($|\psi_j|^2$) in Fig. 2(d) for the states marked by the red plus sign in Fig. 2(b). It can be seen that the edge states are concentrated on the two

edges of leg a. The bulk-boundary correspondence can be properly established by linking a bulk topological invariant in the momentum space under periodic boundary conditions to the edge states under open boundary conditions. In Fig. 2(b), we plot the invariant quantity in terms of a winding number ν (red circles) defined by the formula

$$\nu = \frac{1}{\pi} \int_0^{2\pi} i\langle u_k|\partial_k u_k\rangle dk, \quad (2)$$

where $|u_k\rangle$ stands for the filled Bloch band and k denotes a quasimomentum. It turns out that the gapped phase before (after) the critical point corresponds to $\nu = 1$ (0), which indicates a clear topological phase transition, and the correspondence between the bulk and the boundary.

The single-particle orbitals discussed above can be filled one by one from the lowest energy onwards to obtain different ground-state phases arising at different fillings of fermions in the many-body context. Fundamentally, hardcore bosons share some properties with the spinless fermions such as the energy and diagonal correlations, but strictly in one dimension. The situation is different in the case of a two-leg ladder. A critical study on this front has been performed in Ref. [63], where the differences between noninteracting spinless fermions and hardcore bosons in a two-leg ladder model with uniform leg hopping have been highlighted. It has been shown in Ref. [63] that at half filling, both spinless fermions and hardcore bosons stabilize to the gapped phases as a function of the rung hopping. In these gapped phases, the particles prefer to localize on the rungs. However, the difference between fermions and hardcore bosons is that the transition to the gapped phase occurs after a critical t_p for the case of spinless fermions, whereas for hardcore bosons, the system becomes a gapped RMI phase for any finite value of t_p, indicating a clear difference between the two systems. While these differences exist, the single-particle analysis provides a broad basis for understanding topological insulators in both fermionic and bosonic systems.

In our studies, we show that for the model under consideration, the hardcore bosons in the many-body limit exhibit different phases, such as topological bond order (BO) phases, rung-Mott insulators (RMI), plaquette order (PO) phases, along with superfluid (SF) phases at incommensurate fillings. We first discuss the scenario without interaction ($V = 0$) and then with interaction ($V \neq 0$) for both the cases of uniform and staggered dimerizations.

IV. MANY-BODY PHASES

Interacting bosons in periodic lattices exhibit a range of rich phenomena [68]. One such phenomenon is the phase transition from the gapless superfluid (SF) to gapped Mott insulator (MI) phase at integer filling [69–71]. While the SF-MI transition has been extensively studied in all three dimensions, in one-dimensional lattices, the SF phase is characterized by off-diagonal quasi-long-range order. In the presence of strong on-site interaction, i.e., in the hardcore limit, the system reaches the Tonk's limit [72]. Such hardcore bosons in one dimension mimic the physics of spin-polarized fermions and, therefore, the physics of the associated many-body problem can be extracted from the single-particle picture. One of
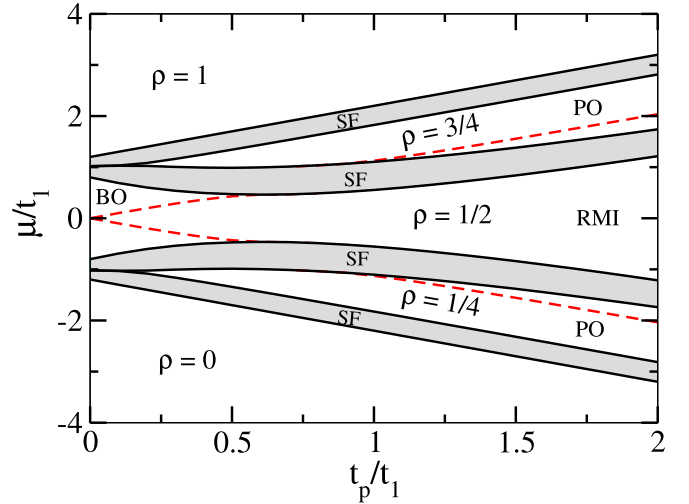

FIG. 3. Phase diagram of model (1) with $V = 0$, $t_a = t_b = 0.6t_1$, and $\alpha_a = \alpha_b = 0.4t_1$ plotted in the t_p-μ plane. The solid black lines show the phase boundaries of gapped phases, such as the plaquette order (PO), the bond order (BO), and the rung-Mott insulator (RMI) phases. The dashed red lines denote the midgap states. The gapless superfluid (SF) phase is represented by the gray shaded area.

the simplest examples is the one-dimensional bosonic SSH model, which exhibits a topological phase transition in the presence of interaction [23–25]. However, in the case of quasi-one-dimensional (quasi-1D) lattices, this mapping is not straightforward and therefore it is difficult to predict the physical picture of a many-body problem.

In this section, we analyze the many-body physics of the SSH ladder shown in Eq. (1) in the absence of interaction (i.e., $V = 0$) for both of the cases of dimerizations considered here.

A. Uniform dimerization

In Fig. 3, we show the phase diagram for uniform dimerization on both of the legs of the ladder with $t_a = t_b = 0.6t_1$ and $\alpha_a = \alpha_b = 0.4t_1$. The phase diagram is obtained as a function of the chemical potential μ and t_p, and it exhibits three gapped phases at $\rho = 1/2$, $1/4$, and $3/4$, denoted by the white regions with black solid boundaries. The boundaries of these gapped phases are calculated using the formula

$$\mu_- = E(N) - E(N-1), \quad \mu_+ = E(N+1) - E(N), \quad (3)$$

where $E(N)$ is the ground-state energy of the system consisting of N bosons. Here, μ_- (μ_+) is the chemical potential that defines the lower (upper) boundary of a gapped phase. All the lines in the figure are plotted after extrapolating the values of $\mu_\pm$ to the thermodynamic limit. One of the major differences that appears in the energy gap at $\rho = 1/2$ as compared to the single-particle picture is that it always remains finite as a function of t_p [compare with Fig. 2(a)]. A similar feature exists for the nondimerized hardcore bosonic ladder where a gapped RMI phase extends until $t_p = 0$ at half filling, in contrast to the single-particle physics [63]. The red dashed lines are the midgap edge states, which are determined by analyzing the ρ-μ plot, as shown in Fig. 4. The figure depicts the behavior of the bulk (ρ_b) and edge (ρ_e) densities, which
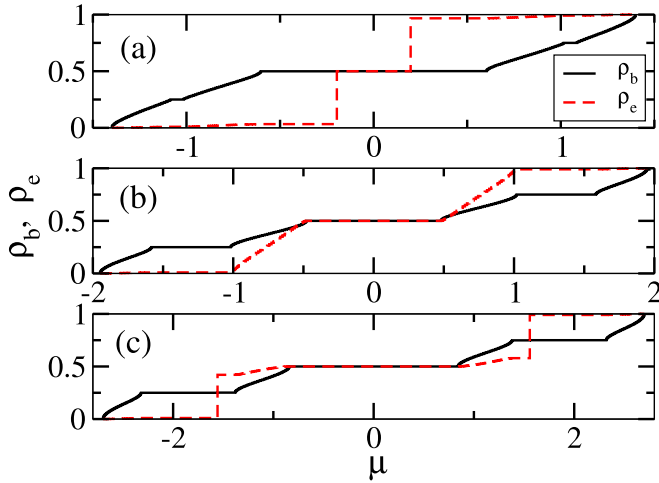
FIG. 4. The figure displays the bulk and edge densities of the system represented by ρ_b and ρ_e, respectively, as a function of μ. (a)–(c) The ρ_b (solid lines) and ρ_e (dashed lines) with varying chemical potential μ for $t_p = 0.2t_1$, $0.75t_1$, and $1.5t_1$, respectively, corresponding to three cuts in the phase diagram shown in Fig. 3. This shows the nature of the bulk phases (gapped or gapless) when the edge states are being filled in different parameter regimes.

are defined as

$$\rho_b = \frac{1}{L-2} \sum_{j=2}^{L-1} \langle n_{aj} + n_{bj} \rangle \tag{4}$$

and

$$\rho_e = \frac{1}{4} \langle n_{a1} + n_{b1} + n_{aL} + n_{bL} \rangle, \tag{5}$$

respectively, as a function of μ. Figures 4(a)–4(c) show the ρ-μ behavior for $t_p = 0.2t_1$, $0.75t_1$, and $1.5t_1$, respectively, corresponding to three different cuts in the phase diagram of Fig. 3. The plateaus in the ρ_b curves (black solid lines) indicate the three bulk gaps at $\rho = 1/4$, $\rho = 1/2$, and $\rho = 3/4$, which confirm the existence of the gapped phases. The shoulders around the plateaus are the signature of gapless regions where the system exhibits a superfluid (SF) character with off-diagonal quasi-long-range order. The behavior of the ρ_e (red dashed lines) in Fig. 4 reflects the existence of edge states in the system. When the bulk is gapped, the sudden change in the number of particles at the edges (N_e) by two or a change in ρ_e by 0.5 for $t_p = 0.2t_1$ and $1.5t_1$ [Figs. 4(a) and 4(c)] mark the μ of the midgap edge states. The change in N_e by two particles is due to the two degenerate midgap edge states at that particular μ. Interestingly, for the case of $t_p = 0.75t_1$ [Fig. 4(b)], ρ_e increases continuously only when the bulk is in the gapless SF region with density $1/4 < \rho_b < 1/2$ and $1/2 < \rho_b < 3/4$. This indicates that the edge states get filled up while the bulk of the system exhibits a gapless SF phase. As discussed earlier, a similar phenomenon can be seen in the single-particle case, where the edge states survive inside the bands between half and quarter fillings.

Now we discuss the properties of the gapped phases in different parameter regimes. At $\rho = 1/2$, when $t_p = 0$, the two chains are isolated SSH chains. Due to the dimerized hopping on both legs, the system exhibits a gapped bond order
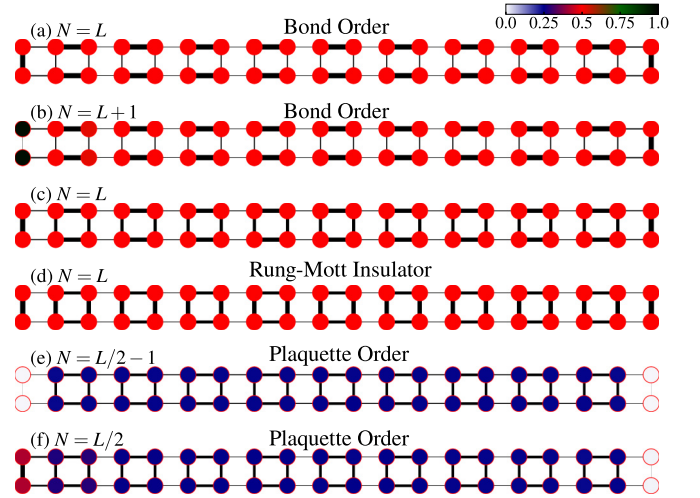

FIG. 5. The figure shows the bond energies (B_j) of all the bonds defined in Eq. (6) and the on-site particle number ($\langle n_j \rangle$) for different phases corresponding to Fig. 3 with a system consisting of 40 sites ($L = 20$ rungs). In the figures, the thickness of a bond is proportional to the respective strength of B_j, and the face color of the circles represents the values of $\langle n_j \rangle$. This captures different dimerization patterns and the existence of edge states in different phases. (a) B_j and $\langle n_j \rangle$ corresponding to the bond order (BO) phase at 1/2 filling ($N = L$) for $t_p = 0.2t_1$, which has two filled edge states (localized at each edge). The parameters in (b) are the same as (a), but with $N = L + 1$, which has three occupied edge states (two localized on the left edge and one on the right edge). (c),(d) The same quantities for $t_p = 0.75t_1$ and $1.5t_1$, respectively, at 1/2 filling ($N = L$). The change in bond order pattern can be seen going from (a) the bond order (BO) to (d) the rung-Mott insulator (RMI) phase. (e),(f) The 1/4-filling plaquette order (PO) phases for parameters $t_p = 0.5t_1$ with $N = L/2 - 1$ and $t_p = 1.5t_1$ with $N = L/2$, respectively. The edge state appears (localized on the left edge) in (f). Note that in all the cases, we have used a small on-site potential of $-0.001t_1$ in one edge to break the degeneracy of the edge-state pair.

(BO) phase along the legs with edge states on both legs. For the other limit of t_p, when it is large compared to the hopping along the legs, the system is gapped once again, but due to the dimerization along the rungs. This phase is known as the rung-Mott insulator (RMI) phase, as already introduced before. However, from the phase diagram shown in Fig. 3, it can be seen that the two gapped phases at two limits of t_p are connected without any gap closing. To identify these phases, we calculate the bond energy along the legs and the rungs using the formula given by

$$B_{a,j} = \langle a_j^\dagger a_{j+1} + \text{H.c.} \rangle, \quad B_{b,j} = \langle b_j^\dagger b_{j+1} + \text{H.c.} \rangle,$$
$$B_{r,j} = \langle a_j^\dagger b_j + \text{H.c.} \rangle. \tag{6}$$

Here the subscripts a, b, and r denote the leg a, leg b, and rung, respectively. Figures 5(a)–5(d) display the bond energy in all the bonds, along with the on-site particle densities for a system of size $L = 20$ at half filling when $t_p = 0.2t_1$, $0.2t_1$, $0.75t_1$, and $1.5t_1$, respectively. Here the thickness of the bonds is proportional to the bond energy B_j, and the face color of the circles represents the particle densities on a particular site. In Fig. 5(a), we can see that the alternate bonds along the

legs are stronger, indicating the BO phase with one particle delocalized in the first and last rungs. When both of the legs are isolated ($t_p = 0$), a configuration with one particle in one of the edges of leg a and one particle in one of the edges of leg b is an energetically favorable configuration at half filling. However, in Fig. 5(a), since we consider a finite rung hopping ($t_p = 0.2t_1$), the system chooses to be in a state such that both of the edge rungs have one particle delocalized in them, which is the minimum energy configuration. We can get more insight regarding the edge states by moving away from half filling, e.g., by adding one extra particle to the system, we get a strong bond on the rightmost rung, as shown in Fig. 5(b). This is because at $\rho_b = 1/2$, there are, in principle, two pairs of edge states at different μ. Since in this case we consider $N = L + 1$ particles, three out of four edge states are filled. Due to this, two particles reside on the left edge of the ladder (i.e., the first rung) and one particle resides on the right edge of the ladder (i.e., the last rung). The particle that resides on the last rung delocalizes itself on the rung due to finite t_p [as can be seen from Fig. 5(b)].

Apart from the gapped phase at $\rho = 1/2$, we also see two more gapped phases at $\rho = 1/4$ and $3/4$, which is expected from the single-particle analysis. Note that the gapped phases at $\rho = 1/4$ and $\rho = 3/4$ are dual to each other due to the particle-hole symmetric nature of the model in the absence of interaction ($V = 0$). At $\rho = 1/4$ ($\rho = 3/4$), for $t_p = 0$, the system is in the SF phase, but when t_p is strong, a particle (hole) tends to get localized in every alternate plaquette of the ladder and hops within the plaquette only. This phase is very similar to the BO phase, but here a particle gets trapped in a plaquette rather than a bond, which we call the plaquette order (PO) phase. In Figs. 5(e) and 5(f), we show the bond energy and particle densities of the gapped phase at $\rho = 1/4$ for $t_p = 0.5t_1$ and $1.5t_1$, respectively. Here we can see that at every alternate plaquette, the bond energy is stronger. But the edge state exists only in Fig. 5(f), which is dimerized in the first rung.

This analysis clearly shows that the strong topological character ceases to appear in the case of uniform dimerization and the zero-energy edge states become midgap edge states for any finite value of t_p, hence ruling out any topological phase transition as a function of t_p. However, in the following, we show that the case of staggered dimerization exhibits a clear topological phase transition, even in the presence of finite interaction.

B. Staggered dimerization

In this case, the leg a (leg b) of the ladder is considered to be of a topological (trivial) nature. Similar to the uniform dimerization case, we first discuss the many-body phase diagram in the absence of interaction ($V = 0$) and compare it with the single-particle picture [Fig. 2(b)]. In Fig. 6, we show the phase diagram with the parameters $t_a = t_b = 0.6t_1$ and $\alpha_a = -\alpha_b = 0.4t_1$ in the $\mu - t_p$ plane. In the figure, the white regions bounded by the black line with circles correspond to the gapped phases, and the gray regions around them are the gapless regions. The phase diagram clearly shows a phase transition between two gapped phases as a function of t_p at half filling. In the following, we show that this
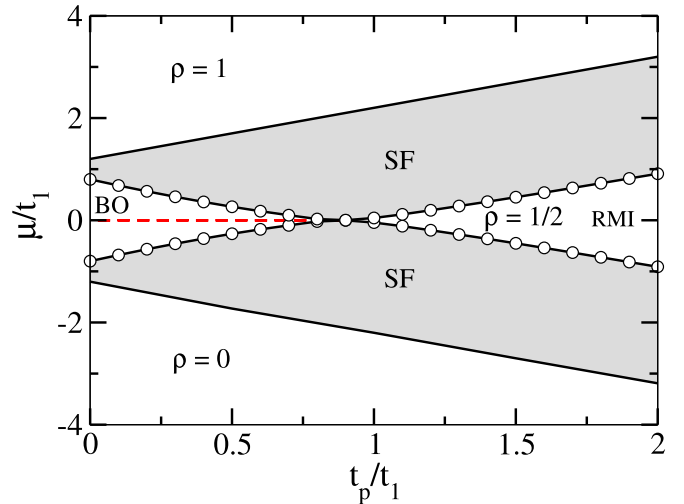

FIG. 6. Phase diagram of model (1) with $V = 0$, $t_a = t_b = 0.6t_1$, and $\alpha_a = -\alpha_b = 0.4t_1$ is plotted in the t_p-μ plane. The solid black lines show the phase boundaries of gapped phases and the dashed lines denote the midgap states. The gapless superfluid (SF) phase is represented by the shaded gray area. A topological phase transition happens through a gap-closing point for $\rho = 1/2$ from a topological bond order (BO) to a trivial rung-Mott insulator (RMI) phase.

transition through a gap-closing point is a well-defined topological phase transition, which was already indicated in the single-particle picture [compare with Fig. 2(b)].

First of all, when $t_p = 0$, the system corresponds to two isolated SSH chains. Due to staggered dimerization, the upper leg at $\rho = 1/2$ exhibits a topological BO phase with zero-energy edge states, and the lower leg exhibits a trivial BO phase without any edge states. Because of this, there exists a finite gap at $t_p = 0$ with zero-energy states at the middle. Upon switching on the rung hopping t_p, the system shows an affinity towards dimerizing along the rungs due to the enforcement of the RMI character. As a result, the topological BO phase and the edge states (red dashed line) survive up to certain values of t_p. After a critical value of $t_p \sim 0.9t_1$, the dimerization in the rungs dominates, leading to the appearance of the gapped RMI phase, which does not exhibit any edge states. This transition clearly occurs through a gap-closing point, indicating a topological phase transition as a function of t_p. These two gapped phases can be distinguished by comparing their bulk behavior through B_j, as shown in Figs. 7(a) and 7(b) which are plotted for parameters $t_p = 0.25t_1$ and $1.5t_1$, respectively, at $\rho = 1/2$. From the figure, it can be seen that when t_p is below the critical value, the dimerization is maximum along the legs of the ladder and the left edge of leg a is occupied by a particle, indicating the presence of an edge state. When t_p is above the critical value, we see a dominant dimerization along the rungs forming the RMI phase, which does not host any edge states.

To inspect the gap-closing point, we analyze the behavior of the single-particle correlation function $\Gamma_{ij} = \langle a_i^\dagger a_j \rangle$ as a function of the distance $|i - j|$ at half filling for three different values of t_p lying in both the gapped phases as well as at the gap-closing point. From Fig. 8, it can be seen that when the system lies in the topological BO phase for $t_p = 0.25t_1$, the correlation Γ_{ij} decays exponentially (red squares), indicating
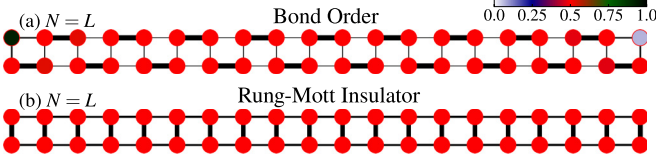
FIG. 7. The figure shows the bond energy (B_j) of all the bonds defined in Eq. (6) and the on-site particle number ($\langle n_j \rangle$) for different phases of a system consisting of 40 sites ($L = 20$). (a),(b) Two gapped phases at the 1/2 filling ($N = L$), which are topological bond order (BO) and trivial rung-Mott insulator (RMI) phases corresponding to the parameter value $t_p = 0.25t_1$ and $1.5t_1$, respectively, in Fig. 6. Here the thickness of a bond is proportional to the corresponding value of B_j, and the face color of the circles represents the on-site particle number. We can see the change in dimerization pattern between (a), which also has an occupied edge state (localized at the left edge), and (b). Note that in both cases, we have used a small on-site potential of $-0.001t_1$ in one edge to break the degeneracy of the edge-state pair.

the gapped nature of the phase. Similar features can be seen for the RMI phase for $t_p = 1.5t_1$ (green circles). However, near the gap-closing point i.e., for $t_p = 0.87t_1$ (black diamonds), Γ_{ij} exhibits a power-law decay. Such a behavior of the correlation function indicates that the system becomes a superfluid with quasi-long-range order at the critical point of topological phase transition.

At this point, it is evident that the staggered dimerization case favors a topological phase transition in the many-body limit, which is absent in the case of uniform dimerization. In the remaining part of the paper, we focus on the role of interaction on the topological character displayed by the many-body system in the staggered dimerization case.

V. INTERACTION-INDUCED TOPOLOGICAL PHASE TRANSITION

In this section, we study the fate of the topological phase that occurs for the staggered dimerization case in the presence
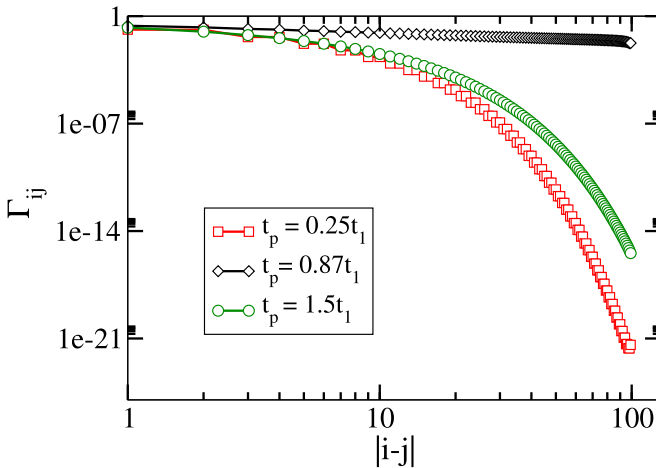

FIG. 8. The figure shows the correlation function Γ_{ij} as a function of distance $|i - j|$ for $V = 0$, $t_p = 0.25t_1$ (red squares), $t_p = 0.87t_1$ (black diamonds), and $t_p = 1.5t_1$ (green circles). Here we show the behavior only along the leg a for a ladder with 200 lattice sites (i.e., $L = 100$).
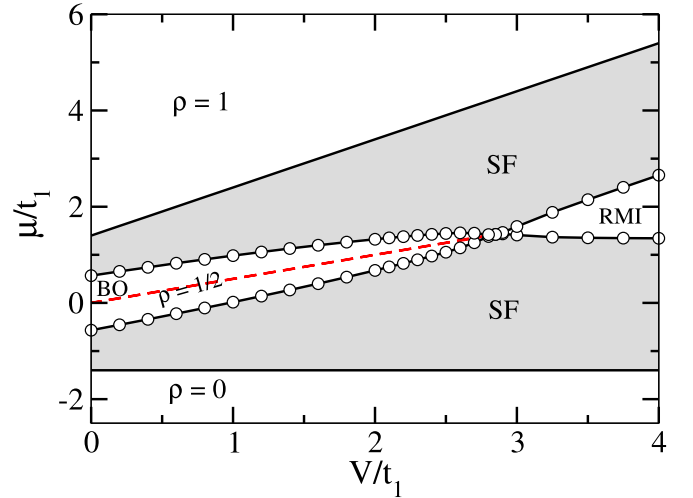

FIG. 9. Phase diagram of model (1) with $t_a = t_b = 0.6t_1$, $\alpha_a = -\alpha_b = 0.4t_1$, and $t_p = 0.2t_1$ plotted in the V-μ plane. The solid black lines show the phase boundaries of gapped phases and the red dashed lines stand for the midgap edge states. The gapless superfluid (SF) phase is represented by the shaded gray area. Here, at $\rho = 1/2$, the topological phase transition occurs from a topological bond order (BO) to a trivial rung-Mott insulator (RMI) phase through a gap-closing point with increasing V.

of interaction (V). For this purpose, we start in the parameter domain $t_p = 0.2t_1$, $t_a = t_b = 0.6t_1$, and $\alpha_a = -\alpha_b = 0.4t_1$ in the noninteracting phase diagram shown in Fig. 6, where the system is in a gapped BO phase exhibiting edge states at $\rho = 1/2$, and examine the effect of finite V. By introducing V, we obtain a phase diagram, which is shown in Fig. 9, in the $\mu - V$ plane, obtained after appropriate finite-size extrapolation. The phase diagram clearly shows a gapped to gapped phase transition, where the gapped and gapless phases are indicated by the white and gray regions, respectively. We find that the degenerate edge states still survive at finite V (indicated by the red dashed line), preserving the topological nature of the phase. With increase in V, however, a gap-closing transition to a trivial phase occurs at a critical interaction strength $V_c \sim 2.85t_1$. The gap-closing transition induced by interaction signifies the bulk-edge correspondence of the topological phase transition, even though the edge states shift from the $\mu/t_1 = 0$ value due to the particle-hole symmetry breaking of the Hamiltonian. Note that in this case, the gapped phase below V_c is a topological BO phase, and above V_c, it is the RMI phase.

The underlying mechanism of this interaction-induced topological phase transition can be described by the arguments based on the minimization of the ground-state energy. Starting from the noninteracting ($V = 0$) case [e.g., Fig. 7(a)], the dimerization pattern reveals a large probability of finding two particles on a single rung. At finite V, this configuration is unfavorable due to an extra energy cost. In such a situation, to minimize the energy, the system tends to dimerize along the rungs by localizing one particle at each rung. This preference of dimerization along the rungs by the particles leads to a transition from the topological BO phase to the RMI phase (trivial) as a function of V. This also suggests that a finite $V > 0$ favors a topological phase transition and, therefore,
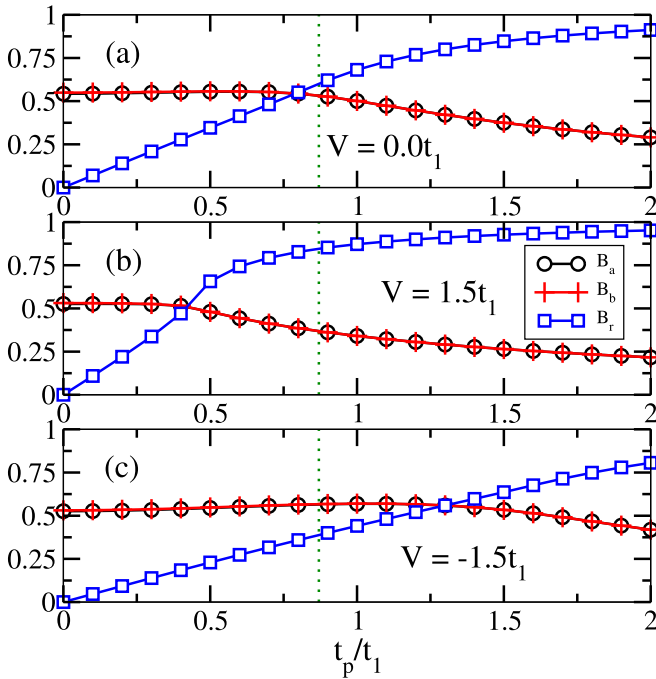
FIG. 10. Bond energies along the legs ($B_{a,b}$) and along the rung (B_r) computed by averaging over all the respective bonds for 240 sites ($L = 120$) at $\rho = 1/2$. (a)–(c) The bond energies for $V = 0.0t_1$, $1.5t_1$, and $-1.5t_1$, respectively, with varying t_p. The B_r dominates over $B_{a,b}$ after different t_p values for different values of V, implying the onset of a trivial RMI phase with different critical transition points. The green dotted lines in all the plots mark the critical point corresponding to $V = 0.0t_1$ in Fig. 6.

the transition should occur at a smaller t_p as compared to the $V = 0$ case. This is confirmed in our numerical simulations, as shown in Fig. 10, where we compare the average bond energies along the legs (B_a and B_b) and the rungs (B_r) as a function of t_p for different values of V. It can be clearly seen that for $V = 1.5t_1$ [Fig. 10(a)], the bond energy along the rungs starts to dominate over the bond energies along the legs at a smaller t_p, indicating an early topological BO-RMI transition compared to the case when $V = 0.0t_1$ [see Fig. 10(b)].

In this context, we also examine the effect of attractive interaction on the topological phase transition. We find that the B_r dominates over all other bond energies at a larger value of t_p for attractive V, as shown in Fig. 10(c) (for $V = -1.5t_1$). This opposite behavior can be understood using an argument similar to the repulsive V case. When $V < 0.0t_1$, the particles prefer to dimerize along the legs rather than on the rungs. Hence, a larger t_p is necessary to break the bond ordering along the legs and introduce rung dimerization as compared to the repulsive V case. These behaviors can also be seen in the phase diagrams shown in Figs. 11(a) and 11(b) for $V = 1.5t_1$ and $V = -1.5t_1$, respectively. Comparing the transition point for $V = 0.0t_1$, marked by vertical dotted lines, we can clearly see that the topological phase transition occurs at a smaller (larger) critical t_p for repulsive (attractive) V.

Another aspect to understand these phase transitions can be the way the interleg interaction modifies the energetics of the system. For example, when $V = 0.0t_1$, the chemical potentials
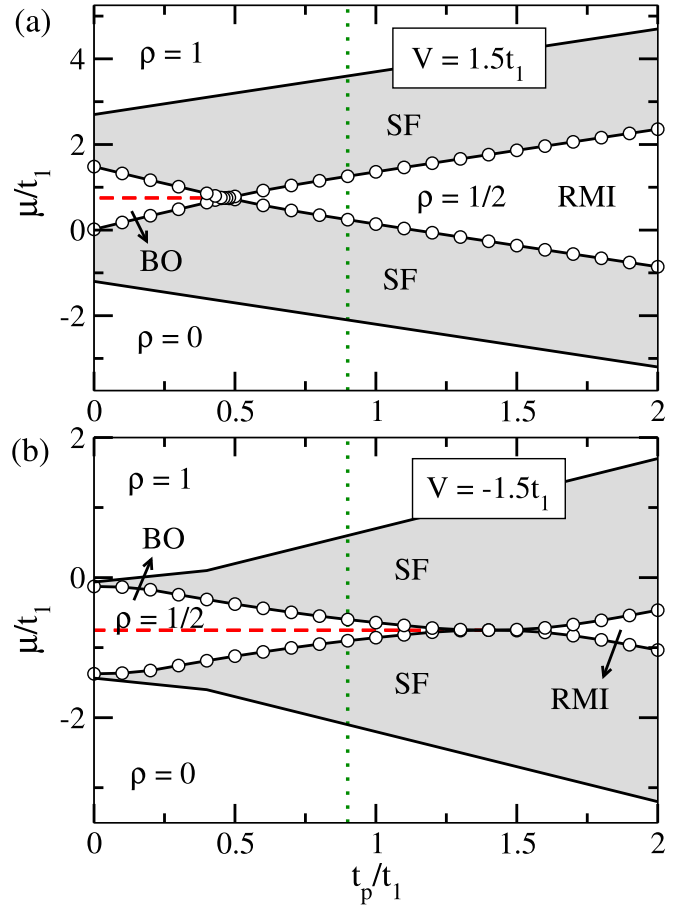

FIG. 11. Phase diagrams of model (1) with (a) $V = 1.5t_1$ and (b) $V = -1.5t_1$ are plotted in the t_p-μ plane. The solid black lines show the phase boundaries of the gapped topological bond order (BO) phase and trivial rung-Mott insulator (RMI) phases. The dashed lines stand for the midgap edge states. The gapless superfluid (SF) phase is represented by the shaded gray area. The green dotted line marks the critical point corresponding to $V = 0.0t_1$ in Fig. 6. The change in the gapless critical points for finite interaction can be seen by comparing to the noninteracting case at half filling.

μ_+ and μ_- are symmetric around $\mu = 0$. On the other hand, when $V = 1.5t_1$, the chemical potentials are modified and the overall phase diagram shifts by $0.75t_1$ [compare the red dashed lines in Figs. 6 and 11(a)]. This is exactly $V/2$ because the two lattice sites in each rung experience an interaction equal to V. However, the critical point shifts to a lower value for a repulsive V. This can actually be understood from the bond energy (B_j) analysis in Fig. 8, where we observe that the bond energies along the legs $B_{a/b,j}$ remains constant up to the gap-closing critical point, after which it decreases. Conversely, the bond energy along the rungs $B_{r,j}$ keeps increasing with increase in t_p and dominates $B_{a/b,j}$. This crossing between the bond energy along the legs and that along the rungs occurs at a lower t_p for $V > 0.0t_1$.

To quantify the interaction-induced topological phase transition, we obtain the critical rung hopping strengths t_p^c for different values of V by monitoring the bulk gap-closing point (as already done for Figs. 6 and 11). To this end, we fix $t_a = t_b = 0.6t_1$ and $\alpha_a = -\alpha_b = 0.4t_1$ in the Hamiltonian
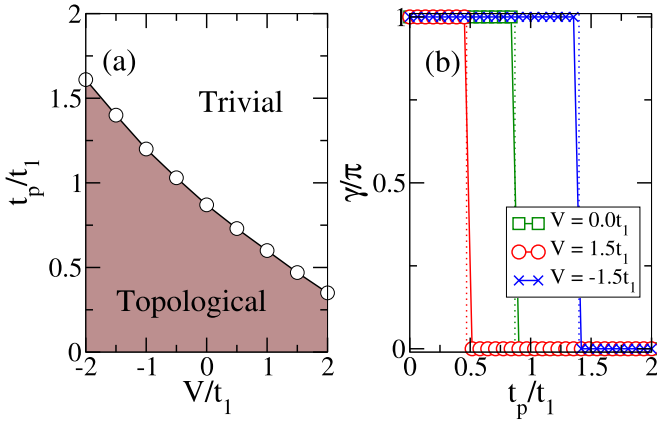
FIG. 12. (a) Phase diagram at $\rho = 1/2$ corresponding to the Hamiltonian given in Eq. (1) for $t_a = t_b = 0.6t_1$ and $\alpha_a = -\alpha_b = 0.4t_1$ (staggered dimerization). Here the topological (trivial) phase is the BO (RMI) phase. The figure shows how the critical point changes with the interaction strength V. (b) Berry phase under twisted phase boundary conditions showing the topological phase transition as a function of t_p/t_1 for $V = 0.0t_1, 1.5t_1$, and $-1.5t_1$ on a system of length $L = 6$ (12 lattice sites). The dotted lines mark the transition points extracted from the phase diagram in (a) corresponding to each V.

shown in Eq. (1) and compute the phase diagram in the $V - t_p$ plane, as shown in Fig. 12(a) where the topological phase (brown region) and trivial phase (white region) are separated by the critical boundary (line with circles). We obtain that the t_p^c shifts to a higher (lower) value for attractive (repulsive) interaction. It is interesting to note that attractive V favors a topological phase from a trivial phase for a range of values of t_p/t_1. For example, starting from $t_p/t_1 = 1$ and $V = 0$, if we move by making V more and more attractive, the system undergoes a trivial to topological phase transition at $V_c \sim -0.5$.

The topological phase transitions can also be detected from the discontinuous jump in the topological invariant of the corresponding phases. A bulk topological invariant, calculated from the Berry phase, is always linked with the symmetry-protected edge states according to bulk-boundary correspondence in topological systems. The Berry phase, defined by the formula

$$\gamma = \int_0^{2\pi} \langle \psi(\theta) | \partial_\theta \psi(\theta) \rangle d\theta, \tag{7}$$

can be a suitable topological invariant for our model in the many-body limit under twisted phase boundary conditions (TBCs) [24,25,73]. Here, $|\psi\rangle$ is the ground-state wave function, and we achieve the TBC by setting $a_j \rightarrow e^{i\theta/L} a_j$ and $b_j \rightarrow e^{i\theta/L} b_j$ in leg a and leg b, respectively. When the twist angle θ is varied from 0 to 2π adiabatically, $|\psi\rangle$ picks up a phase, which is simply the Berry phase. Thus, γ is expected to be quantized in units of π for a topological phase, whereas it should vanish in the trivial phase. We plot γ/π as a function of t_p in Fig. 12(b) to capture the topological phase transitions for $V = 0.0t_1, 1.5t_1$, and $-1.5t_1$. As anticipated, γ clearly distinguishes the topological BO and trivial RMI phases for all three values of V. It also marks the respective critical points ($\sim 0.87t_1$ for $V = 0.0t_1$, $\sim 0.47t_1$ for $V = 1.5t_1$, and $\sim 1.4t_1$ for

$V = -1.5t_1$), where we see an abrupt jump from $\gamma = \pi$ to $\gamma = 0$.

The many-body topological phase diagram in the non-interacting limit (Fig. 6) is qualitatively similar to the single-particle energy spectrum [Fig. 2(b)]. In the presence of interaction, however, the critical point shifts to a different critical rung hopping and the transition in this case is not completely reminiscence of its noninteracting counterpart. For example, the transition for $V < 0.0t_1$ occurs at a larger t_p compared to the $V = 0.0t_1$ case [see the phase diagram in Fig. 12(a)]. Thus, there exists a parameter regime in the phase diagram where a topological phase arises which is not necessarily present for $V = 0.0t_1$ and it is solely an outcome of the interaction.

Thouless charge pumping

We now propose an experimentally relevant quantity in terms of Thouless charge pumping (TCP) [74], which can detect the interaction-induced topological phase transition arising from our model. The TCP has recently been used to characterize the topological nature of a system both in theory and in experiments [13,14,75–83]. As per the TCP measure, it is possible to pump a quantized amount of charge with an adiabatic variation of the system parameters in a pumping cycle which is related to the Chern number. The celebrated Rice-Mele model [84,85] defines the pumping protocol in one dimension where, in the parameter space, the pumping path winds around a gapless singular point [21]. Here the system periodically and adiabatically goes from a nontrivial to trivial phase, and to a nontrivial phase again, by breaking the symmetry that protects the topology in the system. While, originally, the Rice-Mele model described the TCP of noninteracting systems, recently its connection to interacting systems has been proposed in various systems [21,22,24,42,76,86–90]. For our current system under consideration, which exhibits a topological phase transition, we can define a pumping protocol by introducing a symmetry-breaking term such that the pumping path in the parameter space adiabatically winds around the topological phase transition point.

In the following, we present the pumping protocol for the two-leg ladder system with the parametric extension of the model (1), which is given as

$$\mathcal{H}_p(\tau) = -\sum_j [t_a - (-1)^j \alpha_a](a_j^\dagger a_{j+1} + \text{H.c.})$$

$$-\sum_j [t_b - (-1)^j \alpha_b](b_j^\dagger b_{j+1} + \text{H.c.})$$

$$- [t_o + \delta(\tau)] \sum_j (a_j^\dagger b_j + \text{H.c.})$$

$$+ \Delta(\tau) \sum_j [(-1)^j n_{aj} + (-1)^{j+1} n_{bj}]$$

$$+ V \sum_j n_{aj} n_{bj}, \tag{8}$$

where $\delta(\tau) = A_\delta \cos(2\pi\tau)$ changes the hopping dimerization along the rungs and $\Delta(\tau) = A_\Delta \sin(2\pi\tau)$ changes the staggered on-site potential, which breaks the sublattice symmetry.
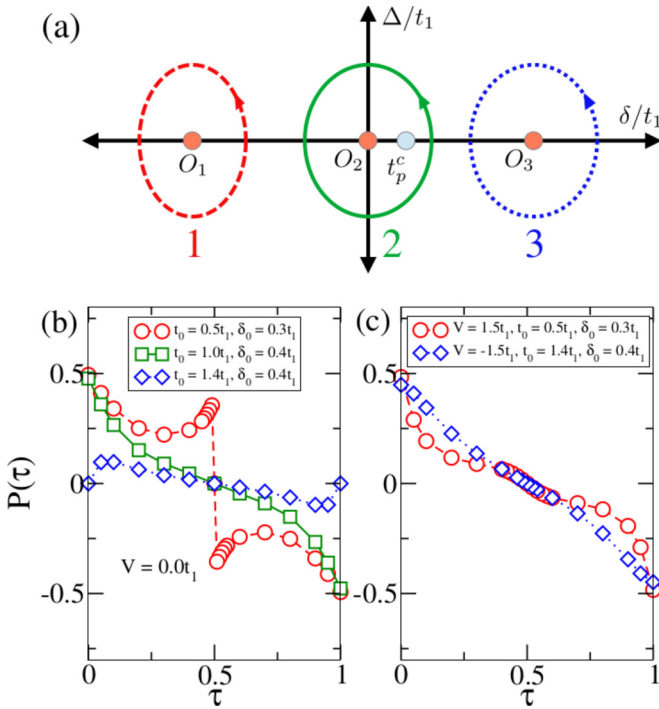
FIG. 13. (a) Pictorial representation of the adiabatic variation of parameters, shown for three different pumping cycles with three different origins (t_o's). The topological phase transition critical point t_p^c is marked with a green circle on the δ axis. (b) The evolution of the polarization [$P(\tau)$] is plotted for three different t_o's corresponding to three different pumping cycles shown in (a) for $V = 0$. Here, $t_p^c \sim 0.87t_1$. Here, only cycle 2, which encloses the t_p^c, shows robust pumping. (c) The evolution of $P(\tau)$ is shown for the same parameters corresponding to cycles 1 and 3 that are considered in (b), but with finite interaction strength $V = 1.5t_1$ and $V = -1.5t_1$, respectively. Unlike the noninteracting case, here a quantized amount of charge is being pumped. We call this phenomenon the interaction-induced topological charge pumping. Here, for all the cases we consider $\Delta = 0.5t_1$ and a finite system of $L = 200$ rungs.

The quantity τ is the adiabatic pumping parameter with $O = (t_p = t_o,\ 0)$ as the origin of the pumping cycle in the $\delta - \Delta$ plane. A schematic representation of the periodic variation of the parameters is shown in Fig. 13(a) for three different t_o's with A_δ and $A_\Delta > 0$. Note that the pumping can only happen if the pumping path encloses the gap-closing critical point (t_p^c). This implies that only for cycle 2 (green continuous line) of Fig. 13(a) can we expect robust and quantized charge pumping.

However, the results obtained for $V = 0$ suggest that the critical rung hopping t_p^c for the topological phase transition can be moved towards smaller and larger values depending on the repulsive or attractive nature of V, respectively. Hence, it can be made possible to shift the t_p^c along the δ axis of Fig. 13(a) by a suitable choice of V such that it lies inside cycle 1 or 3 and a finite quantized amount of pumped charge can be generated in these cases. The phenomenon of charge pumping induced by interactions can be termed an interaction-induced topological charge pumping (iTCP).

In our analysis, the iTCP is demonstrated by defining three different pumping cycles for three parameter

sets of (t_o, A_δ, A_Δ) in Fig. 13(a), such as cycle 1 ($0.5t_1$, $0.3t_1$, $0.5t_1$), cycle 2 ($1.0t_1$, $0.4t_1$, $0.5t_1$), and cycle 3 ($1.4t_1$, $0.4t_1$, $0.5t_1$). All the cycles correspond to the parameter sets $t_a = t_b = 0.6t_1$, $\alpha_a = -\alpha_b = 0.4t_1$, for which the critical rung hopping for the noninteracting ($V = 0$) topological phase transition is $t_p^c \sim 0.87t_1$ (Fig. 6) at half filling. Following the standard protocol of the charge pump, we compute a quantity known as polarization using the formula

$$P(\tau) = \frac{1}{L}\sum_{j=0}^{L-1}\langle\psi(\tau)|(j - L/2)n_j|\psi(\tau)\rangle, \qquad (9)$$

which can estimate the pumped charge (Q) as

$$Q = \int_0^1 d\tau\,\partial_\tau P(\tau). \qquad (10)$$

Here, $|\psi(\tau)\rangle$ is the ground state corresponding to the Hamiltonian $\mathcal{H}_p(\tau)$ since the evolution is adiabatic. In Fig. 13(b), we plot $P(\tau)$ for $V = 0$, for the pumping cycle 1 (dashed line with circles), cycle 2 (continuous line with squares), and cycle 3 (dotted line with diamonds). According to the parameters considered here, the t_p^c resides on the δ axis within cycle 2 ($t_o - A_\delta < 0.87t_1 < t_o + A_\delta$) only. Thus, we can see from the figure that only for cycle 2 does $P(\tau)$ varies continuously from 0.5 to -0.5 resulting in $|Q| = 1$. However, for cycle 1 and cycle 3, the situation is completely different. For cycle 1, there is a clear breakdown of charge pumping in the middle of the pumping cycle, and there is no charge being pumped for cycle 3.

To verify the iTCP, we re-perform the pumping along cycles 1 and 3 with finite interactions $V = 1.5t_1$ and $-1.5t_1$, which shift the t_p^c into cycle 1 and cycle 3, respectively. In Fig. 13(c), we plot $P(\tau)$ for cycle 1 (dashed line with circles) and cycle 3 (dotted line with diamonds). The continuous change of $P(\tau)$ from 0.5 to -0.5 clearly shows a quantized TCP for both of the cases. Note that this finite TCP was not present for the $V = 0$ case [Fig. 13(b)] and is induced by the interaction (V), indicating an iTCP. This analysis substantiates the interaction-induced topological phase transition as already shown in Fig. 12.

From the analysis above, we can see that interaction favors a topological phase transition from topological BO to the trivial RMI phase. The same underlying physics also dictates the change in the critical rung hopping of a topological phase transition in the presence of interaction. Such an interaction effect on the topological phase transition allows for an interaction-induced topological charge pumping.

VI. SUMMARY AND OUTLOOK

In summary, we have studied the topological properties of the bosonic Su-Schrieffer-Heeger ladder for its two possible configurations. These configurations correspond to the uniform dimerization case where the dimerization pattern is such that both of the legs are topological for the appropriate choice of boundary conditions, and the staggered dimerization case, where one of the legs is topological and the other is trivial. Compared to previous studies of either single-particle physics or fermions, we analyzed hardcore bosons hopping on the ladder and endowed with interleg interactions. We first analyzed

the ground-state properties of the many-body system without any interleg interaction and showed that for the uniform dimerization case, there is no topological phase transition as a function of the rung hopping strength. Rather, the system goes from a gapped bond order phase to a gapped rung-Mott insulator phase at half filling without any gap closing. In contrast, the staggered dimerization case supports a well-defined topological phase transition from a topological bond order phase to a trivial rung-Mott insulator phase. Further, we investigated the effect of interleg interaction which greatly influences the topological phases. We found a topological phase transition as a function of interaction for a fixed rung hopping strength. We also found that when interaction is fixed, the critical rung hopping for the topological phase transition strongly depends on the nature of the interaction. That is, for repulsive (attractive) interaction, the topological phase transition occurs at a smaller (larger) critical rung hopping strength. We characterized the transitions through multiple approaches and density matrix renormalization group (DMRG) techniques; these included obtaining the excitation gap, edge-state profiles, Berry phases, and Thouless charge pumping measures.

As these studies are performed on hardcore bosons hopping on the SSH ladder and under the influence of interleg interactions, there is scope for extensive further studies. To name a few, the phase diagram warrants a more careful characterization. A highlight feature of bosons is their ability to host superfluidity; further studies could deviate from half filling to study the entry from the superfluid phase into the topological insulating phases. While DMRG provides a tractable technique for deriving properties of the phase diagram, alternative ways of incorporating the effects of interaction, such as Luttinger liquid treatment, would shed light on the nature of the phase transitions and the relevance of various coupling terms. As for the derived measures, Thouless charge pumping is new in the context of interacting bosons and warrants further analysis. Lastly, generalizations of this bosonic SSH ladder model would include deviations from the hardcore constraint to finite on-site interaction strength, multiple legs of the ladder, inhomogeneity stemming from a spatially varying site potential, and frustration due to modified lattice structure. Another extension can be to study the effect of intraleg nearest-neighbor interactions on the topological phase transitions in the system, which is presently under investigation.

Along with more extensive theoretical study, the bosonic SSH ladder system is poised to be explored in experiment. Several ultracold-atomic systems have characterized single bosonic SSH chains and topological phases in optical lattice systems in real space as well as in momentum space [17], employing time-of-flight [12], mean chiral displacement [91], and Thouless pumping [13,14] measures to identify topological features. These avenues would be amenable to studies of interacting ladders, with topological properties directly measurable, for instance, through Rydberg atoms [48]. Mechanical systems [60] have also realized SSH ladders in regimes where simple harmonic approximations hold; going beyond could introduce the equivalent of interactions in the relevant degrees of freedom. Wave-guide arrays, photonic crystals, and superconducting Josephson circuits have all come far in the context of lattice-based, strongly correlated physics, and would be highly amenable to the system at hand. The SSH bosonic ladder would therefore offer rich ground for theory and experiment to go hand in hand.

[1] W. P. Su, J. R. Schrieffer, and A. J. Heeger, Phys. Rev. Lett. **42**, 1698 (1979).

[2] A. J. Heeger, S. Kivelson, J. R. Schrieffer, and W. P. Su, Rev. Mod. Phys. **60**, 781 (1988).

[3] J. K. Asbóth, L. Oroszlány, and A. Pályi, The Su-Schrieffer-Heeger (SSH) model, in *A Short Course on Topological Insulators: Band Structure and Edge States in One and Two Dimensions* (Springer International, Cham, 2016), pp. 1–22.

[4] N. Batra and G. Sheet, Resonance **25**, 765 (2020).

[5] T. Senthil, Annu. Rev. Condens. Matter Phys. **6**, 299 (2015).

[6] L. Fidkowski and A. Kitaev, Phys. Rev. B **83**, 075103 (2011).

[7] Z.-C. Gu and X.-G. Wen, Phys. Rev. B **80**, 155131 (2009).

[8] F. Pollmann, A. M. Turner, E. Berg, and M. Oshikawa, Phys. Rev. B **81**, 064439 (2010).

[9] X. Chen, Z.-C. Gu, Z.-X. Liu, and X.-G. Wen, Science **338**, 1604 (2012).

[10] J. K. Pachos and S. H. Simon, New J. Phys. **16**, 065003 (2014).

[11] K. von Klitzing, Nat. Phys. **13**, 198 (2017).

[12] M. Atala, M. Aidelsburger, J. T. Barreiro, D. Abanin, T. Kitagawa, E. Demler, and I. Bloch, Nat. Phys. **9**, 795 (2013).

[13] S. Nakajima, T. Tomita, S. Taie, T. Ichinose, H. Ozawa, L. Wang, M. Troyer, and Y. Takahashi, Nat. Phys. **12**, 296 (2016).

[14] M. Lohse, C. Schweizer, O. Zilberberg, M. Aidelsburger, and I. Bloch, Nat. Phys. **12**, 350 (2016).

[15] S. Mukherjee, A. Spracklen, M. Valiente, E. Andersson, P. Öhberg, N. Goldman, and R. R. Thomson, Nat. Commun. **8**, 13918 (2017).

[16] L. Lu, J. D. Joannopoulos, and M. Soljačić, Nat. Photon. **8**, 821 (2014).

[17] E. J. Meier, F. A. An, and B. Gadway, Nat. Commun. **7**, 13986 (2016).

[18] T. Kitagawa, M. A. Broome, A. Fedrizzi, M. S. Rudner, E. Berg, I. Kassal, A. Aspuru-Guzik, E. Demler, and A. G. White, Nat. Commun. **3**, 882 (2012).

[19] M. Leder, C. Grossert, L. Sitta, M. Genske, A. Rosch, and M. Weitz, Nat. Commun. **7**, 13112 (2016).

[20] S. Rachel, Rep. Prog. Phys. **81**, 116501 (2018).

[21] A. Hayward, C. Schweizer, M. Lohse, M. Aidelsburger, and F. Heidrich-Meisner, Phys. Rev. B **98**, 245148 (2018).

[22] M. Nakagawa, T. Yoshida, R. Peters, and N. Kawakami, Phys. Rev. B **98**, 115147 (2018).

[23] S. Mondal, S. Greschner, and T. Mishra, Phys. Rev. A **100**, 013627 (2019).

[24] S. Greschner, S. Mondal, and T. Mishra, Phys. Rev. A **101**, 053630 (2020).

[25] F. Grusdt, M. Höning, and M. Fleischhauer, Phys. Rev. Lett. **110**, 260405 (2013).

[26] D. Wang, S. Xu, Y. Wang, and C. Wu, Phys. Rev. B **91**, 115118 (2015).

[27] L. Barbiero, L. Santos, and N. Goldman, Phys. Rev. B **97**, 201115(R) (2018).

[28] B. Sbierski and C. Karrasch, Phys. Rev. B **98**, 165101 (2018).

[29] G. Magnifico, D. Vodola, E. Ercolessi, S. P. Kumar, M. Müller, and A. Bermudez, Phys. Rev. D **99**, 014503 (2019).

[30] J. Sirker, M. Maiti, N. P. Konstantinidis, and N. Sedlmayr, J. Stat. Mech. (2014) P10032.

[31] T. Jin, P. Ruggiero, and T. Giamarchi, Phys. Rev. B **107**, L201111 (2023).

[32] A. M. Marques and R. G. Dias, Phys. Rev. B **95**, 115443 (2017).

[33] X.-L. Yu, L. Jiang, Y.-M. Quan, T. Wu, Y. Chen, L.-J. Zou, and J. Wu, Phys. Rev. B **101**, 045422 (2020).

[34] M. Yahyavi, L. Saleem, and B. Hetényi, J. Phys.: Condens. Matter **30**, 445602 (2018).

[35] G. Salerno, M. Di Liberto, C. Menotti, and I. Carusotto, Phys. Rev. A **97**, 013637 (2018).

[36] M. Di Liberto, A. Recati, I. Carusotto, and C. Menotti, Eur. Phys. J.: Spec. Top. **226**, 27512762 (2017).

[37] X. Zhou, J.-S. Pan, and S. Jia, Phys. Rev. B **107**, 054105 (2023).

[38] A. M. Marques and R. G. Dias, J. Phys.: Condens. Matter **30**, 305601 (2018).

[39] S. Mondal, A. Padhan, and T. Mishra, Phys. Rev. B **106**, L201106 (2022).

[40] F. D. M. Haldane, Phys. Rev. Lett. **50**, 1153 (1983).

[41] E. G. Dalla Torre, E. Berg, and E. Altman, Phys. Rev. Lett. **97**, 260401 (2006).

[42] S. Mondal, S. Greschner, L. Santos, and T. Mishra, Phys. Rev. A **104**, 013315 (2021).

[43] T. Yoshida, I. Danshita, R. Peters, and N. Kawakami, Phys. Rev. Lett. **121**, 025301 (2018).

[44] B.-T. Ye, L.-Z. Mu, and H. Fan, Phys. Rev. B **94**, 165167 (2016).

[45] Y. Kuno, Phys. Rev. B **99**, 064105 (2019).

[46] A. Montorsi, U. Bhattacharya, D. González-Cuadra, M. Lewenstein, G. Palumbo, and L. Barbiero, Phys. Rev. B **106**, L241115 (2022).

[47] S. Julià-Farré, D. González-Cuadra, A. Patscheider, M. J. Mark, F. Ferlaino, M. Lewenstein, L. Barbiero, and A. Dauphin, Phys. Rev. Res. **4**, L032005 (2022).

[48] S. de Léséleuc, V. Lienhard, P. Scholl, D. Barredo, S. Weber, N. Lang, H. P. Büchler, T. Lahaye, and A. Browaeys, Science **365**, 775 (2019).

[49] N. H. Le, A. J. Fisher, N. J. Curson, and E. Ginossar, npj Quantum Inf. **6**, 24 (2020).

[50] C. Li, S. Lin, G. Zhang, and Z. Song, Phys. Rev. B **96**, 125418 (2017).

[51] S. Cheon, T.-H. Kim, S.-H. Lee, and H. W. Yeom, Science **350**, 182 (2015).

[52] X. Li, E. Zhao, and W. Vincent Liu, Nat. Commun. **4**, 1523 (2013).

[53] K. Padavić, S. S. Hegde, W. DeGottardi, and S. Vishveshwara, Phys. Rev. B **98**, 024205 (2018).

[54] S. Santra, A. Agarwala, and S. Bhattacharjee, Phys. Rev. B **103**, 195134 (2021).

[55] D. Bercioux, O. Dutta, and E. Rico, Annal. Phys. **529**, 1600262 (2017).

[56] P. Matveeva, T. Hewitt, D. Liu, K. Reddy, D. Gutman, and S. T. Carr, Phys. Rev. B **107**, 075422 (2023).

[57] M. Jangjan and M. V. Hosseini, Phys. Rev. B **106**, 205111 (2022).

[58] M. Jangjan and M. V. Hosseini, Sci. Rep. **10**, 14256 (2020).

[59] M. Jangjan and M. V. Hosseini, Sci. Rep. **11**, 12966 (2021).

[60] K. Qian, D. J. Apigo, K. Padavić, K. H. Ahn, S. Vishveshwara, and C. Prodan, Phys. Rev. Res. **5**, L012012 (2023).

[61] A. A. Nersesyan, Phys. Rev. B **102**, 045108 (2020).

[62] S.-L. Zhang and Q. Zhou, Phys. Rev. A **95**, 061601(R) (2017).

[63] F. Crépin, N. Laflorencie, G. Roux, and P. Simon, Phys. Rev. B **84**, 054517 (2011).

[64] S. R. White, Phys. Rev. Lett. **69**, 2863 (1992).

[65] U. Schollwöck, Rev. Mod. Phys. **77**, 259 (2005).

[66] S. Rommer and S. Östlund, Phys. Rev. B **55**, 2164 (1997).

[67] U. Schollwöck, Ann. Phys. **326**, 96 (2011).

[68] I. Bloch, J. Dalibard, and W. Zwerger, Rev. Mod. Phys. **80**, 885 (2008).

[69] M. P. A. Fisher, P. B. Weichman, G. Grinstein, and D. S. Fisher, Phys. Rev. B **40**, 546 (1989).

[70] D. Jaksch, C. Bruder, J. I. Cirac, C. W. Gardiner, and P. Zoller, Phys. Rev. Lett. **81**, 3108 (1998).

[71] M. Greiner, O. Mandel, T. Esslinger, T. W. Hänsch, and I. Bloch, Nature (London) **415**, 39 (2002).

[72] B. Paredes, A. Widera, V. Murg, O. Mandel, S. Fölling, I. Cirac, G. V. Shlyapnikov, T. W. Hänsch, and I. Bloch, Nature (London) **429**, 277 (2004).

[73] L. Lin, Y. Ke, and C. Lee, Phys. Rev. B **107**, 125161 (2023).

[74] D. J. Thouless, Phys. Rev. B **27**, 6083 (1983).

[75] R. Citro and M. Aidelsburger, Nat. Rev. Phys. **5**, 87 (2023).

[76] C. Schweizer, M. Lohse, R. Citro, and I. Bloch, Phys. Rev. Lett. **117**, 170405 (2016).

[77] Y. E. Kraus, Y. Lahini, Z. Ringel, M. Verbin, and O. Zilberberg, Phys. Rev. Lett. **109**, 106402 (2012).

[78] L. Taddia, E. Cornfeld, D. Rossini, L. Mazza, E. Sela, and R. Fazio, Phys. Rev. Lett. **118**, 230402 (2017).

[79] A.-S. Walter, Z. Zhu, M. Gächter, J. Minguzzi, S. Roschinski, K. Sandholzer, K. Viebahn, and T. Esslinger, Nat. Phys. **19**, 1471 (2023).

[80] L. Wang, M. Troyer, and X. Dai, Phys. Rev. Lett. **111**, 026802 (2013).

[81] L. Lin, Y. Ke, and C. Lee, Phys. Rev. A **101**, 023620 (2020).

[82] Y. Ke, J. Zhong, A. V. Poshakinskiy, Y. S. Kivshar, A. N. Poddubny, and C. Lee, Phys. Rev. Res. **2**, 033190 (2020).

[83] Y. Ke, X. Qin, Y. S. Kivshar, and C. Lee, Phys. Rev. A **95**, 063630 (2017).

[84] M. J. Rice and E. J. Mele, Phys. Rev. Lett. **49**, 1455 (1982).

[85] J. K. Asbóth, L. Oroszlány, and A. Pályi, Adiabatic charge pumping, Rice-Mele model, in *A Short Course on Topological Insulators: Band Structure and Edge States in One and Two Dimensions* (Springer International, Cham, 2016), pp. 55–68.

[86] E. Berg, M. Levin, and E. Altman, Phys. Rev. Lett. **106**, 110405 (2011).

[87] E. Bertok, F. Heidrich-Meisner, and A. A. Aligia, Phys. Rev. B **106**, 045141 (2022).

[88] S. Mondal, E. Bertok, and F. Heidrich-Meisner, Phys. Rev. B **106**, 235118 (2022).

[89] Y.-T. Lin, D. M. Kennes, M. Pletyukhov, C. S. Weber, H. Schoeller, and V. Meden, Phys. Rev. B **102**, 085122 (2020).

[90] Y. Kuno and Y. Hatsugai, Phys. Rev. Res. **2**, 042024(R) (2020).

[91] D. Xie, W. Gou, T. Xiao, B. Gadway, and B. Yan, npj Quantum Inf. **5**, 55 (2019).